Monthly Notices of the ROYAL ASTRONOMICAL SOCIETY

MNRAS **463,** 1968–1979 (2016) doi:10.1093/mnras/stw2145
Advance Access publication 2016 August 25

# On the faint-end of the high-$z$ galaxy luminosity function

Bin Yue,[1]★ Andrea Ferrara[1,2] and Yidong Xu[3]

[1]*Scuola Normale Superiore, Piazza dei Cavalieri 7, I-56126 Pisa, Italy*
[2]*Kavli IPMU (WPI), Todai Institutes for Advanced Study, the University of Tokyo, 5-1-5 Kashiwanoha, Kashiwa 277-8583, Japan*
[3]*Key Laboratory for Computational Astrophysics, National Astronomical Observatories, Chinese Academy of Sciences, Beijing 100012, China*

Accepted 2016 August 23. Received 2016 August 23; in original form 2016 April 5

## ABSTRACT

Recent measurements of the luminosity function (LF) of galaxies in the Epoch of Reionization (EoR, $z \gtrsim 6$) indicate a very steep increase of the number density of low-mass galaxies populating the LF faint-end. However, as star formation in low-mass haloes can be easily depressed or even quenched by ionizing radiation, a turnover is expected at some faint UV magnitudes. Using a physically motivated analytical model, we quantify reionization feedback effects on the LF faint-end shape. We find that if reionization feedback is neglected, the power-law Schechter parametrization characterizing the LF faint-end remains valid up to absolute UV magnitude $\sim -9$. If instead radiative feedback is strong enough that quenches star formation in haloes with circular velocity smaller than 50 km s$^{-1}$, the LF starts to drop at absolute UV magnitude $\sim -15$, i.e. slightly below the detection limits of current (unlensed) surveys at $z \sim 5$. The LFs may rise again at higher absolute UV magnitude, where, as a result of interplay between reionization process and galaxy formation, most of the galaxy light is from relic stars formed before the EoR. We suggest that the galaxy number counts data, particularly in lensed fields, can put strong constraints on reionization feedback. In models with stronger reionization feedback, stars in galaxies with absolute UV magnitude higher than $\sim -13$ and smaller than $\sim -8$ are typically older. Hence, the stellar age–UV magnitude relation can be used as an alternative feedback probe.

**Key words:** galaxies: high-redshift – cosmology: observations – cosmology: theory – dark ages, reionization, first stars.

## 1 INTRODUCTION

Reionization is one of the most important processes during cosmic history. It starts around $z \sim 30$–$20$,[1] when the first stars begin to form (see reviews e.g. Abel, Bryan & Norman 2002; Ciardi & Ferrara 2005; Bromm et al. 2009), and it is completed by $z \sim 5$–$6$, when virtually all the intergalactic medium (IGM) is ionized (Becker et al. 2001; Fan, Carilli & Keating 2006; Ouchi et al. 2010; Stark et al. 2010). A deeper understanding of the reionization process relies on observations of its driving sources that are generally believed to be high-$z$ normal star-forming galaxies (Lorenzoni et al. 2011; Salvaterra, Ferrara & Dayal 2011; Finkelstein et al. 2012; Jaacks et al. 2012; Robertson et al. 2013, 2015). So far, observations of high-$z$ LFs have reached absolute UV magnitude $\sim -13$ (at $z \sim 6$) and redshift up to $\sim 10$ (McLure et al. 2013; Oesch et al. 2014; Bouwens et al. 2015a,b; Finkelstein et al. 2015; Roberts-Borsani et al. 2016) thanks to the deepest HUDF/XDF surveys (Bouwens et al. 2011; Ellis et al. 2013; Illingworth et al. 2013; Oesch et al. 2013) and gravitational lensing magnification (Atek et al. 2015; Livermore, Finkelstein & Lotz 2016; McLeod, McLure & Dunlop 2016). Recent observations of high-$z$ galaxies are reviewed in Finkelstein (2015).

The observed high-$z$ galaxies are mostly the brightest ones among reionization sources. However, in the hierarchical structure formation scenario, massive haloes form through a series of mergers of smaller progenitors. Such small haloes are more numerous and dominate the collapsed matter fraction budget. Thus, it is natural to expect that more faint galaxies exist, hosting most of the stellar mass and dominating the ionizing photon budget (e.g. Choudhury & Ferrara 2007).

A problem might arise with the above scenario. Sustaining star formation requires continuous cold gas supply, but the available gas content in haloes could be limited by various feedback effects, namely supernova feedback and radiative feedback. Both supernova

★E-mail: bin.yue@sns.it

[1] This is the typical redshift when the $3\sigma$ fluctuations of the cosmic density field on the molecular hydrogen cooling mass scale collapse to form haloes, see Barkana & Loeb (2001). The very early and rare first stars can form from fluctuations $>3\sigma$ at much higher redshifts (Naoz, Noter & Barkana 2006; Trenti & Stiavelli 2007).

explosions and ionizing radiation inject thermal energy into the interstellar medium, interrupting the gas cooling process. However, the internal feedback due to stars is self-regulated since a decreasing star formation efficiency also reduces the feedback strength. Thus, feedback operates more efficiently when it is driven by ionizing radiation from external sources (nearby galaxies and/or a background). External ionizing photons could completely quench the star formation by either heating the cosmic gas and reducing the efficiency of gas accretion, or by continuously evaporating the gas already contained in haloes. These processes are collectively referred to as 'reionization feedback' as they occur during the Epoch of Reionization (EoR). The effects mainly depend on the gravitational potential of individual haloes, and are particularly evident in smaller galaxies. If reionization feedback is indeed effective, a significant decline in the abundance of galaxies with the lowest luminosities is expected (Wise et al. 2014; O'Shea et al. 2015). It follows that the role played by faint galaxies as reionization sources might be questioned.

The shape of the luminosity function (LF) faint-end during EoR is expected to carry signatures of the star formation modulation imposed by impinging ionizing radiation. However, compared with the wealth of detailed theoretical studies on how external ionizing radiation suppresses star formation in galaxies (see e.g. Sobacchi & Mesinger 2013a,b), there are fewer predictions on the LF of high-$z$ galaxies in the full absolute magnitude range, including the faint/low-mass galaxies most sensitive to reionization feedback. This is clearly due to the limited dynamical range that numerical simulations can achieve. Nevertheless, Gnedin (2016) has numerically investigated the LF down to the faint-end. He found evidence for a deviation of the LF from the Schechter function at absolute UV magnitude $\sim -14$, although the LF continues to rise up to magnitude $\sim -12$. This can be translated into an equivalent sharp cutoff of the Schechter function in the UV magnitude range $\sim -14$ to $\sim -12$ to match the required UV emissivity for completing the reionization (Mitra, Choudhury & Ferrara 2015; Robertson et al. 2015).

Observationally, the minimum mass of host haloes of high-$z$ galaxies has been constrained by Muñoz & Loeb (2011). By assuming that the galaxy stellar mass is gathered in halo growth history through a series of instantaneous star formation bursts triggered by mergers, and comparing the theoretical LFs with deep *HST* surveys, they derived a minimum mass of $\approx 2.5 \times 10^9\,\mathrm{M}_\odot$ at $z \sim 6$–$8$. This minimum mass is consistent with the reionization requirements. Because of the existence of this mass floor, LFs drop gently above a turnover absolute UV magnitude. They also found that the total star formation rate (SFR) in all high-$z$ galaxies is only moderately higher than the SFR contained by already observed galaxies, therefore the star formation activity in ultra-faint galaxies must be heavily suppressed by the reionization feedback (however, for a slightly different view see Salvadori & Ferrara 2009).

Within current detection limits no deviation with respect to the Schechter power law increase has been reported. However, a sensitivity improvement, as provided by, e.g. the Frontier Fields,[2] might change the situation dramatically (Yue et al. 2014). In view of these developments it is therefore timely to develop an analytical model of the high-$z$ galaxy LF matching the already observed bright part of the LF, and simultaneously predicting the faint-end far below the current detection limit. By comparing the predictions with upcoming observations, we may then characterize reionization feedback effects in detail. This task involves various complications, including the metallicity and stellar evolution, and a mass-dependent star formation efficiency. Moreover, the SFR probably depends on other properties of the halo and its environments as well, in addition to the halo mass, as found by simulations (e.g. Pallottini et al. 2014.)

Pioneering works have derived the high-$z$ galaxy properties from the better-known halo properties, using various models to associate the star formation history to the mass assembly history of the host halo (e.g. Choudhury & Ferrara 2007; Trenti et al. 2010; Tacchella, Trenti & Carollo 2013; Wyithe, Loeb & Oesch 2014; Behroozi & Silk 2015; Mason, Trenti & Treu 2015; Mashian, Oesch & Loeb 2016; Sun & Furlanetto 2016). In particular, in a series of works Trenti et al. (2010), Tacchella et al. (2013) and Mason et al. (2015), an analytical method has been developed to calculate the LF of high-$z$ galaxies from the dark matter halo mass function. The main assumption in their approach is that the 'star formation efficiency' – defined as the ratio of gas converted into stars to the accreted *dark matter* mass – is a function of halo mass only, i.e. it is independent of redshift. The redshift dependence of the galaxy luminosity is ascribed to its mass assembly history. Therefore, once the star formation efficiency at a given redshift is obtained, it is assumed to hold at any redshifts. Alternatively, to derive the high-$z$ galaxy LF from halo mass function, a mean redshift-independent SFR–halo mass relation is used in Mashian et al. (2016). Moreover, Behroozi & Silk (2015) assumed that the specific star formation rate is proportional to the specific halo accretion rate. They found that the stellar mass to halo mass ratio evolves rapidly at $z > 4$.

In this paper,[3] we extend the Mason et al. (2015) model by including the reionization feedback effect under various assumptions for the feedback strength, then use it to derive the EoR galaxy LF to below current detection limits. The layout is as follows. In Section 2 we introduce the algorithm to compute LFs from halo mass functions and halo star formation histories. We model the influence of reionization feedback on the galaxy abundance self-consistently. In Section 3 we present our predicted LFs extended to galaxies in which star formation is significantly influenced by reionization feedback effects. We also discuss the SFR–stellar mass relations and the mean stellar age–UV magnitude relations there. Conclusions and discussions are given in Section 4.

## 2 METHOD

### 2.1 From haloes to galaxies

Whether and how a halo contributes to the galaxy LF depends on how efficient it accretes matter and converts accreted matter into stars. Assume that a halo with mass $M_\mathrm{h}$ at redshift $z_0$ collects mass at a rate of $\mathrm{d}M_\mathrm{h}/\mathrm{d}t'$ at cosmic time $t'$, and suppose further that an accreted mass element, $\Delta M'_\mathrm{h} = (\mathrm{d}M_\mathrm{h}/\mathrm{d}t')\mathrm{d}t'$, later on increases the SFR at cosmic time $t$ by $\Delta\mathrm{SFR}(M_\mathrm{h}, t, t') = f(M_\mathrm{h})g(t - t')\Delta M'_\mathrm{h}$, where the star formation efficiency $f(M_\mathrm{h})$ refers to the fraction of accreted mass covered into stars. Following the spirit of Trenti et al. (2010), Tacchella et al. (2013) and Mason et al. (2015), we assume $f(M_\mathrm{h})$ depends only on halo mass $M_\mathrm{h}$, but we introduce an additional mass-independent function $g(t - t')$ to account for

[2] http://www.stsci.edu/hst/campaigns/frontier-fields/

[3] Throughout the paper, we use the *Planck* cosmology parameters (Planck Collaboration XIII 2015): $\Omega_m = 0.308$, $\Omega_\Lambda = 0.692$, $h = 0.6781$, $\Omega_b = 0.0484$, $n = 0.9677$ and $\sigma_8 = 0.8149$. The transfer function is from Eisenstein & Hu (1998).

the time-dependence. Integrating over all accreted matter elements before $t$, we have the SFR of this halo at cosmic time $t$:

$$\mathrm{SFR}(M_\mathrm{h}, t) = \int_{t_f}^{t} f(M_h) g(t - t') \frac{\mathrm{d}M_\mathrm{h}}{\mathrm{d}t'} \mathrm{d}t', \quad (1)$$

where $t_f$ is the cosmic time corresponding to the redshift $z_f$ when this halo formed. An accreted gas element is gradually converted into stars in an 'extended burst', for which the time-dependence can be modelled as (Cen & Ostriker 1992; Gnedin 1996; Chiu & Ostriker 2000; Choudhury & Srianand 2002; Samui, Srianand & Subramanian 2007):

$$g(t - t') = \frac{t - t'}{\kappa^2 t_d^2(z_f)} \exp\left[-\frac{t - t'}{\kappa t_d(z_f)}\right], \quad (2)$$

where

$$t_d(z_f) = \sqrt{\frac{3\pi}{32 G \rho_\mathrm{vir}(z_f)}} \quad (3)$$

is the dynamic time-scale for a halo with mean density $\rho_\mathrm{vir}$, and $\kappa$ is a free parameter that controls the duration of the burst.

Following Tacchella et al. (2013), we only track the halo assembly history back to the half-mass redshift, which is a good approximation as pointed by Mason et al. (2015) (see their fig. 4): for haloes with $M_\mathrm{h} = 10^{11}\,\mathrm{M}_\odot$ at $5 \lesssim z \lesssim 20$, stars formed in progenitors with $M < M_\mathrm{h}/2$ only contribute $\lesssim$1–10 per cent to the total UV luminosity. A further assumption is that the halo mass grows (by accretion and minor mergers) at a constant rate between $z_0$ and $z_f$, i.e.

$$\frac{\mathrm{d}M_\mathrm{h}}{\mathrm{d}t'} = \frac{M_\mathrm{h}}{2(t_0 - t_f)}, \quad (4)$$

where $t_0$ is the cosmic time at redshift $z_0$. Therefore the SFR in this halo can be written as

$$\begin{aligned}\mathrm{SFR}(M_\mathrm{h}, t) &= f(M_h) \frac{M_h}{2(t_0 - t_f)} \int_{t_f}^{t} g(t - t')\,\mathrm{d}t' \\ &= \mathrm{SFR}_\mathrm{M15} \int_{t_f}^{t} g(t - t')\,\mathrm{d}t', \end{aligned} \quad (5)$$

where $\mathrm{SFR}_\mathrm{M15}$ is the SFR used in Mason et al. (2015). Compared with the $\mathrm{SFR}_\mathrm{M15}$, the parameter $\kappa$ in the time-dependent factor $\int_{t_f}^{t} g(t - t')\,\mathrm{d}t'$ introduces a new degree of freedom in the SFR prescription. If $g(t - t')$ is a Dirac delta-function, which means that accreted gas forms stars instantaneously, or $\kappa \ll 1$, or $t - t_f \gg \kappa t_d$, this factor approaches unity and the SFR reduces to $\mathrm{SFR}_\mathrm{M15}$. Nevertheless, $\kappa$ can be constrained only from observations (see below).

At redshift $z_0$, a halo of mass $M_\mathrm{h}$ formed at $z_f$ has a luminosity (e.g. Samui et al. 2007):

$$L(M_\mathrm{h}, z_0, z_f) = \int_{t_f}^{t_0} \mathrm{SFR}(M_\mathrm{h}, t) l_\nu(t_0 - t)\mathrm{d}t, \quad (6)$$

a stellar mass

$$m_\star(M_\mathrm{h}, z_0, z_f) = \int_{t_f}^{t_0} \mathrm{SFR}(M_\mathrm{h}, t) m(t_0 - t)\mathrm{d}t, \quad (7)$$

and a mean stellar age

$$t_\star(M_\mathrm{h}, z_0, z_f) = \frac{1}{m_\star} \int_{t_f}^{t_0} \mathrm{SFR}(M_\mathrm{h}, t) m(t_0 - t)(t_0 - t)\mathrm{d}t. \quad (8)$$

Here $l_\nu(\Delta t)$ is the Single Stellar Populations (SSP) SED template, i.e. the luminosity of an instantaneous star formation burst with unit stellar mass at the time $\Delta t$ after the burst; we always use the luminosity at the wavelength 1600 Å when calculating the absolute UV magnitude. $m(\Delta t)$ is the mass fraction of surviving stars $\Delta t$ after the burst. For both $l_\nu(\Delta t)$ and $m(\Delta t)$ we use the template of Bruzual & Charlot (2003) with Chabrier IMF between 0.1 and 100 $\mathrm{M}_\odot$ and fixed metallicity of $0.02\,\mathrm{Z}_\odot$.

Before deriving the LF of galaxies from halo mass function, we need to obtain the $f(M_h)$ curve. This is determined by comparing the theoretical mean luminosity–halo mass relations with that from observations. From equation (6), haloes with the same mass could have different luminosities if they formed at different redshifts. Given the probability distribution of the formation time, $p(w)$, their mean luminosity is

$$\bar{L}(M_\mathrm{h}, z_0) = \int L(M_\mathrm{h}, z_0, z_f) p(w)\,\mathrm{d}w, \quad (9)$$

where $w$ is related to the formation redshift $z_f$ by

$$w = \sqrt{0.707} \frac{\delta_c(z_f) - \delta_c(z_0)}{\sqrt{\sigma^2(M_h/2) - \sigma^2(M_h)}}, \quad (10)$$

with $\delta_c(z_f)$ being the critical density contrast for spherical collapse at $z_f$ linearly extrapolated to present time, and $\sigma^2(M_h)$ being the variance of density fluctuations smoothed on mass scale $M_h$. In the elliptical collapse scenario the $p(w)$ has the simple expression (Giocoli et al. 2007):

$$p(w) = 2w\,\mathrm{erfc}(w/\sqrt{2}), \quad (11)$$

where erfc is the complementary error function.

On the other hand, a relation between the observed absolute UV magnitude and the halo mass could be constructed by 'abundance matching', i.e. forcing the number density of galaxies with absolute UV magnitude smaller than $M_\mathrm{UV,obs}$ to match the number density of haloes with mass above $M_\mathrm{h}$:

$$\int_{-\infty}^{M_\mathrm{UV,obs}} \Phi_\mathrm{Sch}(M'_\mathrm{UV}, z_0)\mathrm{d}M'_\mathrm{UV} = \int_{M_\mathrm{h}}^{\infty} \frac{\mathrm{d}n_\mathrm{h}}{\mathrm{d}M'_\mathrm{h}} \mathrm{d}M'_\mathrm{h}, \quad (12)$$

where $\Phi_\mathrm{Sch}$ is the Schechter parametrization of the LF (Bouwens et al. 2015a). Here the observed absolute UV magnitude $M_\mathrm{UV,obs}$ corresponds to the dust-attenuated luminosity, which is related to the intrinsic UV magnitude $M_\mathrm{UV}$ by

$$M_\mathrm{UV} = M_\mathrm{UV,obs} - A_{1600}, \quad (13)$$

where $A_{1600}$ is the dust extinction given by (Meurer, Heckman & Calzetti 1999)

$$A_{1600} = 4.43 + 1.99\beta, \quad (14)$$

with $\beta$ being the luminosity-dependent UV spectrum slope. $A_{1600}$ must be $\geq 0$ and $\beta$ is fitted in Bouwens et al. (2014) by a linear form

$$\beta = \beta_0 + \frac{\mathrm{d}\beta}{\mathrm{d}M_0}(M_\mathrm{UV,obs} - M_0), \quad (15)$$

where $M_0 = -19.5$. The best-fitting parameters of a collection of *HST* observations given by Bouwens et al. (2014) are used in this work, i.e. $\beta_0 = (-1.70, -1.85, -1.91, -2.00, -2.05, -2.13)$ and $d\beta/dM_0 = (-0.20, -0.11, -0.14, -0.20, -0.20, -0.15)$ at redshifts $z = (2.5, 3.8, 5.0, 5.9, 7.0, 8.0)$, respectively. At intermediate redshifts we linearly interpolate; for higher redshifts we use the linear extrapolation for $\beta_0$ and fix $\mathrm{d}\beta/\mathrm{d}M_0 = -0.20$. At each $M_h$, by equating $\bar{L}$ with the luminosity of the dust-corrected absolute UV magnitude $M_\mathrm{UV}$, we obtain the $f(M_\mathrm{h})$.

After calibration, we convert the luminosity of the halo into an observed absolute UV magnitude, for which we write its explicit form here for convenience:

$$M_{\rm UV,obs}(M_h, z_0, z_f) =$$

$$\begin{cases} \left(1 - 1.99\frac{{\rm d}\beta}{{\rm d}M_0}\right)^{-1}(M_{\rm UV} - M_0 + 4.43 + 1.99\beta_0) + M_0, \\ \quad ({\rm if}\ M_{\rm UV} < M_0 - \left(1.99\frac{{\rm d}\beta}{{\rm d}M_0}\right)^{-1}(4.43 + 1.99\beta_0)) \\ M_{\rm UV}, \\ \quad ({\rm if}\ M_{\rm UV} \geq M_0 - \left(1.99\frac{{\rm d}\beta}{{\rm d}M_0}\right)^{-1}(4.43 + 1.99\beta_0)), \end{cases} \quad (16)$$

where $M_{\rm UV}$ is the absolute UV magnitude of the luminosity given by equation (6).

Galaxies with the same luminosity could be hosted by haloes with different masses that formed at different redshifts. Among haloes of mass $M_h$, only those formed at a specified redshift, $z_{\rm mag}$, can host galaxies with observed absolute UV magnitude $M_{\rm UV,obs}$; $z_{\rm mag}$ is then obtained by substituting $M_{\rm UV,obs}$, $M_h$ and $z_0$ into equation (16). The LF is then written as

$$\Phi(M_{\rm UV,obs}, z_0) = \int {\rm d}M_{\rm h} \frac{{\rm d}n_{\rm h}}{{\rm d}M_{\rm h}} p(w_{\rm mag}) \frac{{\rm d}w_{\rm mag}}{{\rm d}M_{\rm UV,obs}}, \quad (17)$$

where ${\rm d}n_{\rm h}/{\rm d}M_{\rm h}$ is the halo mass function (Sheth & Tormen 1999; Sheth, Mo & Tormen 2001), and $w_{\rm mag} = w(M_h, z_0, z_{\rm mag})$. The integration is performed over the range of $M_h$ for which a $z_{\rm mag}$ solution exists.

The free parameter $\kappa$ is determined by comparing the derived LF with the observations from Bouwens et al. (2015a). We use a reduced chi-square to measure the deviation of the predicted $\Phi$ from the observations, which is defined as

$$\chi^2_{\rm red}(\kappa) = \frac{1}{n-1}\sum_i \frac{(\Phi - \Phi_i)^2}{\sigma_i^2}, \quad (18)$$

where $\Phi$ is the predicted LFs from equation (17) by using the best-fitting Schechter parametrization of Bouwens et al. (2015a) to calibrate the $f(M_{\rm h})$ (see equation 12), $\Phi_i$ and $\sigma_i$ are observational points of LFs and errors in Bouwens et al. (2015a). The sum is performed on all observational points at redshifts 5, 6, 7 and 8 except for those with upper limits only; $n$ is the number of all points used.

The $\chi^2_{\rm red}$ as a function of $\kappa$ is shown in Fig. 1. We find that the deviation is small and stable at $\kappa \lesssim 0.1$, implying that observations favour a scenario in which the accreted gas is typically converted into stars on a time-scale $\lesssim 0.1 t_d$. We do not find lower limits on the value of $\kappa$. Therefore, we take $\kappa = 0.1$ hereafter. The calibrated $f(M_{\rm h})$ at $z_0 \sim 5$ is plotted in Fig. 2.

To derive the uncertainties in $f(M_{\rm h})$, we randomly sample the three Schechter parameters, $\Phi^*$, $M^*_{\rm UV}$ and $\alpha$, assuming that they all follow a Gaussian distribution with standard deviation equal to the $1\sigma$ error given in Bouwens et al. (2015a). The region containing 68.3 per cent of the $f(M_{\rm h})$ values in each mass bin is plotted in Fig. 2. We do not account for the uncertainties in $\beta_0$ and ${\rm d}\beta/{\rm d}M_0$. We find that the uncertainties are larger for smaller haloes ($\lesssim 10^{10}\,{\rm M}_\odot$), because of the weaker constraints on the faint-end slope of LFs. In the following, we will use the calibration at $z_0 \sim 5$ for all calculations.

### 2.2 Radiative feedback during EoR

We now incorporate the reionization feedback effects into the above modelling of galaxy LF. How reionization feedback affects a halo depends on two separate issues: (a) the probability that the halo is located in ionized bubbles, and (b) how fast the gas supply is interrupted, or its gas photo-evaporated. For a given cosmological evolutionary scenario, (a) is determined by the total amount of emitted ionizing photons and the gas recombination rate. The point (b) is instead determined by complex radiation hydrodynamical processes inside galaxies.

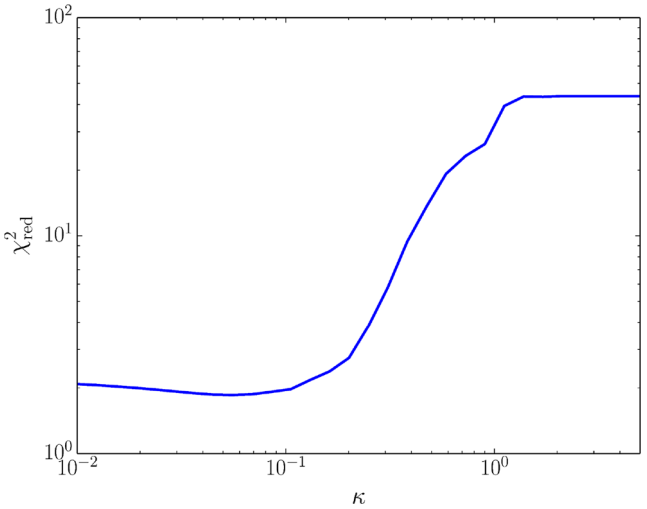


**Figure 1.** The $\chi^2_{\rm red}$ as a function of $\kappa$.

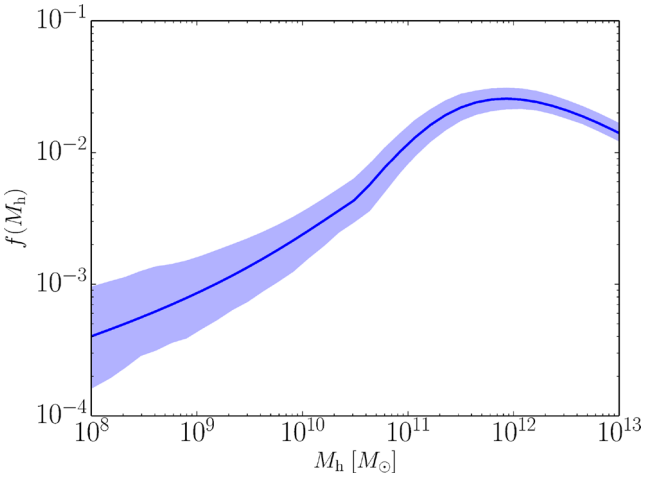


**Figure 2.** The function $f(M_{\rm h})$ calibrated by using the Schechter formula of the observed LF at $z_0 \sim 5$ in Bouwens et al. (2015a) and fix $\kappa = 0.1$. The shaded regions are uncertainties, see the text.

Specifically, we assume that the star formation efficiency $f(M_{\rm h})$ calibrated by matching the theoretical LF to the Schechter function is valid down to the atomic-cooling halo mass (see Appendix A for a check of the supernova feedback effects), unless in these haloes star formation (i) never ignites, or (ii) is totally quenched by the external ionizing radiation. Such events can occur in haloes with circular velocity $v_c$ smaller than a threshold $v_c^*$, further located in ionized bubbles (see e.g. Choudhury & Srianand 2002). Here $v_c$ depends on both $M_{\rm h}$ and $z_f$ (Barkana & Loeb 2001). We note that currently the threshold for quenching star formation by external ionizing radiation is still rather uncertain, and in terms of circular velocity, it varies from $\sim$10 km s$^{-1}$ to $\sim$70 km s$^{-1}$, depending on the intensity and spectrum of the ionizing flux, the time interval in which the halo is exposed to the radiation, self-shielding effects,

and so on (e.g. Thoul & Weinberg 1996; Gnedin 2000; Kitayama et al. 2000; Dijkstra et al. 2004; Sobacchi & Mesinger 2013b).

With star formation being quenched at $z_q$, analogously to equation (6), the emission rate of ionizing photons is

$$\dot{N}_{\rm ion}(M_{\rm h}, z_0, z_q, z_f) = \int_{t_f}^{t_q} {\rm SFR}(M_{\rm h}, t)\dot{q}(t_0 - t){\rm d}t, \quad (19)$$

where the rate $\dot{q}$ is taken from Bruzual & Charlot (2003). Taking into account the reionization feedback, we have three possible star formation histories in haloes with viral temperature $>10^4$ K (we neglect the contribution from minihaloes, as substantial star formation activity in minihaloes is unlikely and rather uncertain).

(i) A halo with $v_c < v_c^*$ can sustain continuous star formation if it is always located outside ionized bubbles.

(ii) A halo with $v_c < v_c^*$ that originally formed in a neutral region later became ionized has its star formation quenched[4] at $z_q$ ($z_0 < z_q < z_f$). In this case the star formation activity only happens between $z_f$ and $z_q$.

(iii) A halo with $v_c > v_c^*$ is massive enough that reionization feedback has no effects on it, no matter whether it is located inside or outside ionized bubbles.

To evaluate reionization feedback we need to know the probability, $\mathcal{P}_b(M_{\rm h}, z)$, that a halo with mass $M_{\rm h}$ is located in an ionized bubble at redshift $z$. This probability is closely related to the volume filling factor of ionized regions $Q_{\rm H\,II}$ at the corresponding redshift. Once the escape fraction of ionizing photons, $f_{\rm esc}$, is assigned, we can compute the evolution of the filling factor of ionized regions

$$\frac{{\rm d}Q_{\rm H\,II}}{{\rm d}t} = f_{\rm esc}\frac{\dot{n}_{\rm ion}}{n_{\rm H}} - Q_{\rm H\,II}^2 C(z) n_{\rm H}(1+z)^3\alpha_{\rm B}, \quad (20)$$

where $\dot{n}_{\rm ion}$ is the ionizing photon emissivity, $n_{\rm H}$ is the comoving total hydrogen number density, $C(z)$ is the clumping factor, and $\alpha_{\rm B}$ is the Case B recombination coefficient. For simplicity we take $T = 10^4$ K for ionized regions, yielding $\alpha_{\rm B} = 2.6 \times 10^{-13}$ cm$^3$s$^{-1}$. We use the form for the clumping factor given by Iliev et al. (2007) normalized to $C = 3.0$ at $z = 5$:

$$C(z) = 6.8345 \times \exp(-0.1822z + 0.003\,505z^2). \quad (21)$$

Taking into account the three cases of star formation history described above, the ionizing photon emissivity can be written as

$$\dot{n}_{\rm ion}(z_0) = \int {\rm d}M_{\rm h}\frac{{\rm d}n_{\rm h}}{{\rm d}M_{\rm h}}\int {\rm d}w\; p(w)\int_{z_f}^{z_0}\dot{N}_{\rm ion}\mathcal{F}(M_{\rm h}, z_q, z_f)\,{\rm d}z_q, \quad (22)$$

where $\mathcal{F}(M_{\rm h}, z_q, z_f)$ is given by

$$\mathcal{F} = \begin{cases} [1 - \mathcal{P}_b(M_{\rm h}, z_0)]\delta(z_q - z_0) + \frac{{\rm d}\mathcal{P}_b}{{\rm d}z_q} & v_c < v_c^* \\ \delta(z_q - z_0) & v_c \geq v_c^* \end{cases} \quad (23)$$

in which $\delta$ is the Dirac delta-function. The term $[1 - \mathcal{P}_b(M_{\rm h}, z_0)]\delta(z_q - z_0)$ corresponds to the case (i), and the terms $\frac{{\rm d}\mathcal{P}_b}{{\rm d}z_q}$ and $\delta(z_q - z_0)$ identify case (ii) and (iii), respectively. To construct a mapping from $Q_{\rm H\,II}$ to $\mathcal{P}_{\rm b}$ we use a method based on the excursion-set formalism (see Appendix B). Once $f_{\rm esc}$ and $v_c^*$ are specified, we numerically solve the differential equation (20) from $z = 20$, when it is safe enough to assume $Q_{\rm H\,II} \approx 0$ and $\mathcal{P}_{\rm B} \approx 0$.

[4] We warn that our treatment here is simplified, as $v_c^*$ might be a function of redshift and intensity of the UV radiation field. We neglect this effect here but refer the interested readers to the discussion in Sobacchi & Mesinger (2013b).

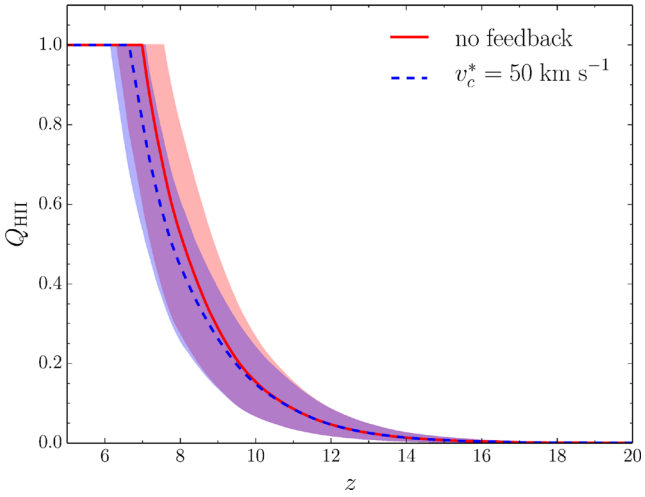


**Figure 3.** The evolution of the filling factor of ionized regions for models without feedback (solid line) and with $v_c^* = 50$ km s$^{-1}$ (dashed line), with the shaded regions being the 68.3 per cent confidence interval. The corresponding e.s. optical depth values are $\tau = 0.063^{+0.009}_{-0.008}$ and $\tau = 0.061^{+0.008}_{-0.007}$, respectively.

Once the ionizing history is determined, the IGM electron scattering optical depth to CMB photons can be derived from

$$\tau = \sigma_{\rm T} n_{\rm H} c\left(1 + \frac{Y_{\rm He}}{4Y_{\rm H}}\right)\int_0^z Q_{\rm H\,II}(z')(1+z')^3\left|\frac{{\rm d}t}{{\rm d}z'}\right|{\rm d}z', \quad (24)$$

where $\sigma_{\rm T} = 6.65 \times 10^{-25}$ cm$^2$ is the cross-section for Thomson scattering, $c$ is the speed of light, $Y_{\rm He} = 0.24$ is the He mass fraction; the H fraction is $Y_{\rm H} = 1 - Y_{\rm He}$; the singly ionized He fraction is assumed to be equal to the HII fraction.

To gain a physical intuition of the effects of feedback on reionization history, in Fig. 3 we compare $Q_{\rm H\,II}(z)$ obtained for a no-feedback model and a strong feedback ($v_c^* = 50$ km s$^{-1}$) model, using a fixed $f_{\rm esc} = 0.2$. We find that the difference between these two models is modest. Adopting a $v_c^* = 50$ km s$^{-1}$ only reduces the Thomson optical depth by $\Delta\tau \approx 0.002$ and delays the reionization by $\Delta z \approx 0.3$.

After including the reionization feedback, the luminosity of a galaxy in which star formation is quenched at $z_q$ ($z_0 < z_q < z_f$) is then

$$L(M_{\rm h}, z_0, z_q, z_f) = \int_{t_f}^{t_q}{\rm SFR}(M_{\rm h}, t)l_\nu(t_0 - t){\rm d}t, \quad (25)$$

where $t_q$ is the quenching time corresponding to redshift $z_q$. This luminosity can be converted into observed absolute UV magnitude by equation (16). The LF including feedback effects is

$$\Phi(M_{\rm UV,obs}, z_0) = \quad (26)$$

$$\int {\rm d}M_{\rm h}\frac{{\rm d}n_{\rm h}}{{\rm d}M_{\rm h}}[1 - \mathcal{P}_b(M_{\rm h}, z_0)]p(w_{\rm mag})I(v_c)\frac{{\rm d}w_{\rm mag}}{{\rm d}M_{\rm UV,obs}}$$
$$+\int {\rm d}M_{\rm h}\frac{{\rm d}n_{\rm h}}{{\rm d}M_{\rm h}}\int_{z_f}^{z_0}{\rm d}z_q\frac{{\rm d}\mathcal{P}_b}{{\rm d}z_q}p(w_{{\rm mag},q})I(v_c)\frac{{\rm d}w_{{\rm mag},q}}{{\rm d}M_{\rm UV,obs}}$$
$$+\int {\rm d}M_{\rm h}\frac{{\rm d}n_{\rm h}}{{\rm d}M_{\rm h}}p(w_{\rm mag})[1 - I(v_c)]\frac{{\rm d}w_{\rm mag}}{{\rm d}M_{\rm UV,obs}}, \quad (27)$$

where, in analogy with the no-feedback case, $w_{{\rm mag},\,q}$ is obtained by substituting $M_h$, $z_0$, $M_{\rm UV,obs}$ and $z_q$ into equation (16). $I$ is

a step function: $I(v_c) = 1$ when $v_c < v_c^*$, and $I(v_c) = 0$ otherwise. The three terms in the above equation correspond to the three cases of star formation history. If $\mathcal{P}_b \equiv 0$ the reionization feedback is not accounted for and the above equation reduces to equation (17).

## 3 RESULTS

### 3.1 Reionization history

We first check whether the Thomson optical depth $\tau$ is consistent with observations in this new scenario. In principle, a higher $f_{\rm esc}$ would promote the reionization process and result in a larger $\tau$. However, it also increases the probability for haloes to be located in ionized bubbles, thus reducing the contribution of ionizing photons from small haloes.

In Fig. 4 we show the completion redshift of reionization, $z_{\rm re}$, and the $\tau$ for different $f_{\rm esc}$ and $v_c^*$ pairs. In each row, the left-hand, central, and right-hand panels show the minimal, best-fitting, and the maximal values allowed by the uncertainty in the star formation efficiency calibration, respectively.

The Thomson optical depth $\tau$ is mainly dependent on $f_{\rm esc}$, but insensitive to $v_c^*$. This is because not all haloes with $v_c < v_c^*$ are sterile, and only those that inhabit ionized bubbles lose the ability to produce ionizing photons. In addition, star formation efficiency in small haloes is low, as seen from Fig. 2. We find that, taking into account the uncertainties in star formation efficiency calibration, the recent *Planck* measurements ($\tau = 0.058 \pm 0.012$, Planck Collaboration XLVII 2016) rule out both the low escape fraction range $f_{\rm esc} \lesssim 0.04$ (see the right-hand panel for $\tau$), and the high escape fraction range $f_{\rm esc} \gtrsim 0.8$ (left-hand panel).

Another interesting problem is whether the conclusion that most ionizing photons come from faint galaxies should be revised once reionization feedback is considered. In Fig. 5 we plot the fractional ionizing photon rate produced in galaxies with absolute UV magnitude above $M_{\rm UV,obs}$, assuming that all galaxies have the same escape fraction of $f_{\rm esc} = 0.2$. It is found that with decreasing redshift, a smaller fraction of ionizing photons comes from fainter galaxies, which is a result of the shallower slope of the LF. When the reionization feedback is taken into account, this fraction is further reduced. However, the qualitative trend remains unchanged. In fact, reionization feedback has significant effects only in the late EoR stages or after EoR, while during the early EoR (e.g. $z \sim 10$) faint galaxies always emit the majority of ionizing photons. We note that this conclusion is based on the assumption of a fixed escape fraction

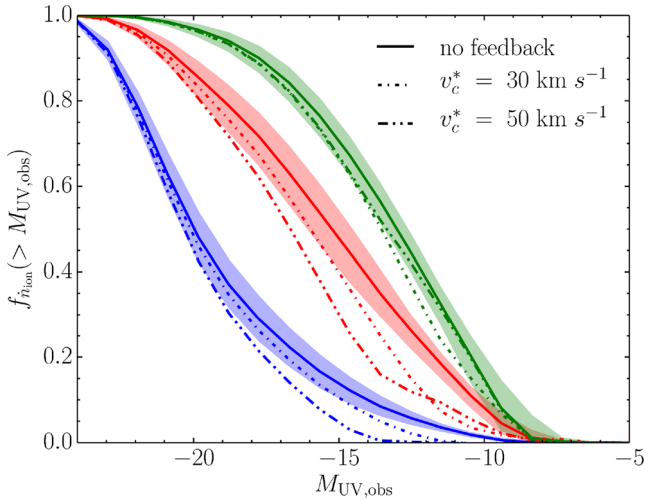


**Figure 5.** Fractional ionizing photon rate from galaxies with absolute UV magnitude above $M_{\rm UV,obs}$, in models with a fixed $f_{\rm esc} = 0.2$, but different $v_c^*$. From top to bottom, each group of curves corresponds to redshift 10, 8, and 5, respectively. To avoid crowding the panel only the 68.3 per cent confidence intervals of the no-feedback model are shown by shaded regions.

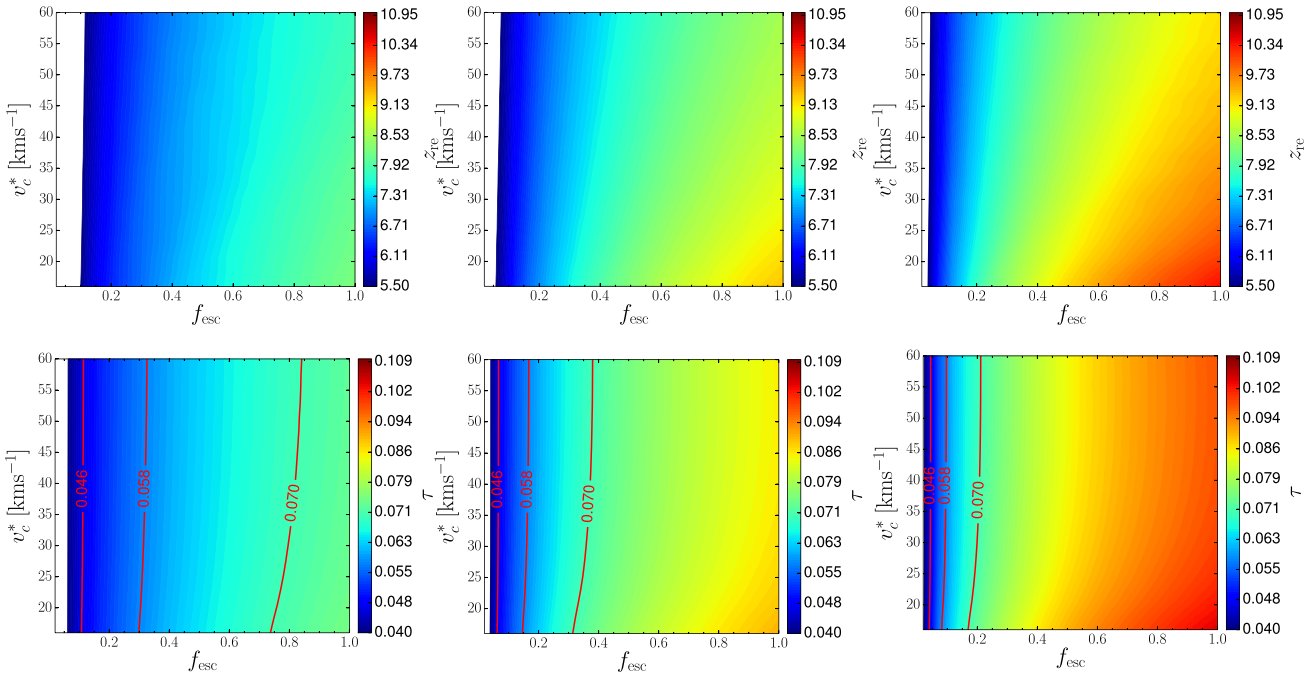


**Figure 4.** The completion redshift of reionization (top row) and the Thomson optical depth (bottom row) as a function of $f_{\rm esc}$ and $v_c^*$. In each row, the left-hand and right-hand panels are the lower and upper limits of the 68.3 per cent confidence intervals; in the middle panel we use best-fitting Schechter parameters in the $f(M_{\rm h})$ calibration. In the bottom panels we mark the *Planck* measurements $\tau = 0.058 \pm 0.012$ (Planck Collaboration XLVII 2016) by lines.

for all galaxies. If smaller galaxies have larger escape fraction (e.g. Ferrara & Loeb 2013), they could have been even more dominant compared to the results shown in Fig. 5.

### 3.2 Feedback imprints on the LF

Next we investigate the effect of reionization feedback on the galaxy LF, and how the LF changes with the feedback strength characterized by the threshold $v_c^*$ and $f_{\rm esc}$. We start by fixing again $f_{\rm esc} = 0.2$, and then predict the resulting LFs at $z_0 = 5$, 6, 7 and 8 for models with $v_c^* = 30$ and 50 km s$^{-1}$. These LFs and the corresponding uncertainties are shown in Fig. 6, where we also plot the LFs for a model with $v_c^*$ corresponding to the atomic-cooling criterion (viral temperature $10^4$ K / $v_c^* = 16$ km s$^{-1}$). This no-feedback model is used as a reference. The observational data from Bouwens et al. (2015a) are also plotted. We find that all LFs match observations in the overlapping magnitude ranges, satisfying our first requirement. In addition, we plot in Fig. 7 the LFs by adopting $v_c^* = 50$ km s$^{-1}$, while $f_{\rm esc}$ equals 0.1 and 0.3, respectively.

In the no-feedback model, the Schechter parametrization (which can be approximated by $\propto 10^{0.4(M_\star - M_{\rm UV,obs})(\alpha+1)}$ for $M_{\rm UV,obs} \gg M_\star$) is valid up to a turnover absolute UV magnitude $M^*_{\rm UV,obs} \sim -9$, above which the number of galaxies drops dramatically. This is because the star formation cannot occur in haloes below the atomic-cooling criterion, whose typical luminosity corresponds to the turnover UV magnitude $M^*_{\rm UV,obs} \sim -9$. Above this atomic-cooling mass, the decrease in the star formation efficiency in low mass haloes is compensated by the increase in the halo number, as seen from Fig. 2, resulting in an LF with a shallower (albeit still negative) slope with respect to the halo mass function.

The reionization feedback distorts the luminosity–halo mass relation, built from the $f(M_h)$ in Fig. 2 (see detailed discussions in Section 3.3), for haloes with $v_c < v_c^*$, resulting in the complex luminosity distributions of faint galaxies hosted by them. We can generally divide the galaxies into two groups: the ones hosted by haloes with $v_c > v_c^*$ and those with $v_c < v_c^*$ respectively. In the former haloes, the star formation activity has never been interrupted. For haloes with $v_c < v_c^*$, many of them were not able to ignite star formation at all, as they formed in ionized patches; the remaining systems could sustain star formation for some time before being quenched by external ionizing radiation. The latter systems are much fainter than the counterparts that have the same mass assembly history in the reference no-feedback model. As a result the number of galaxies drops dramatically above the new turnover UV magnitude $M^*_{\rm UV,obs}$ roughly corresponding the mean luminosity of haloes with $v_c = v_c^*$, namely $M^*_{\rm UV,obs} \approx -12$ ($-15$) for $v_c^* = 30$ (50 km s$^{-1}$).

Galaxies in haloes with $v_c < v_c^*$ (with $M_{\rm UV,obs} > M^*_{\rm UV,obs}$) do not totally disappear. Their number drops down above $M^*_{\rm UV,obs}$, but then rises again for higher absolute UV magnitudes. What causes

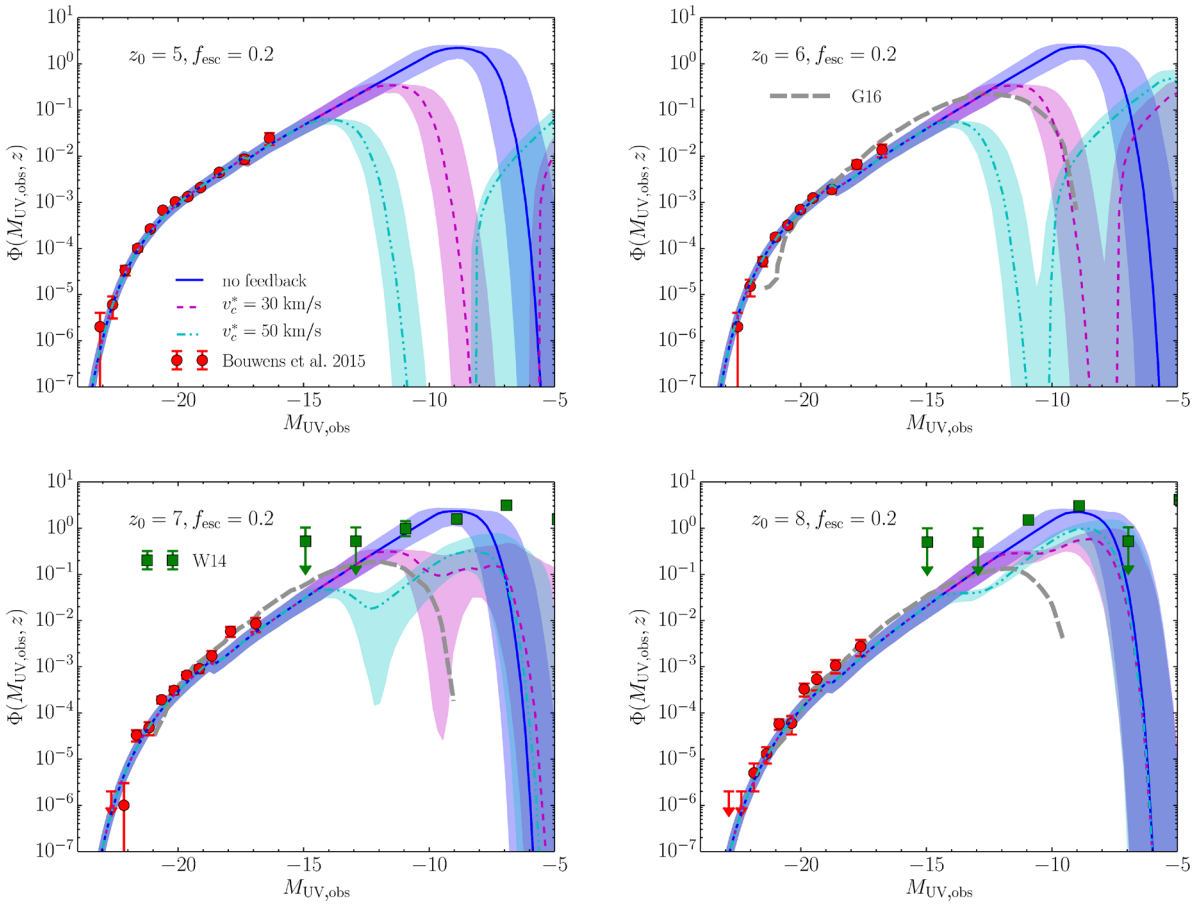


**Figure 6.** The LFs and uncertainties at redshift 5, 6, 7 and 8 for models with varying $v_c^*$. The shaded regions corresponding each of the models are the 68.3 per cent confidence intervals. For comparison, in panels for redshift 6, 7 and 8 we plot the curves in Gnedin (2016) by thick dashed lines (his uncertainties are not shown); in the panels for redshift 7 and 8, we plot the points in Wise et al. (2014) at redshift 7.3 and 8 respectively. Their points with arrows mean there is only one object in the corresponding absolute UV magnitude bin.

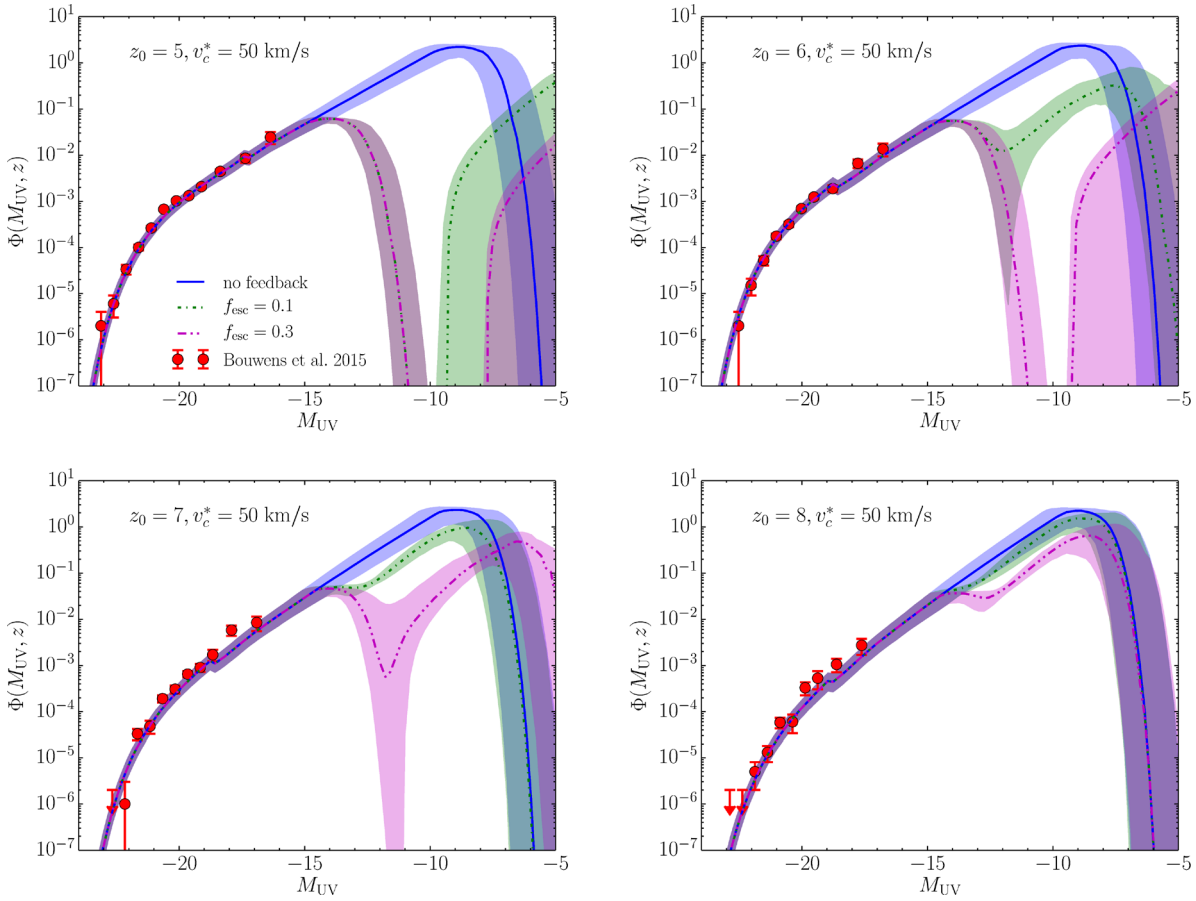


**Figure 7.** Similar to Fig. 6, however here $v_c^* = 50\,\mathrm{km\,s^{-1}}$ while $f_{\rm esc}$ is 0.1 and 0.3, respectively.

the deficit of galaxies just above $M^*_{\rm UV,obs}$? Why, even under strong feedback conditions, the number of faint galaxies remains large (compared to bright galaxies) instead of gradually dropping to zero? The answer to these questions is simple. For haloes with $v_c < v_c^*$, only those formed before the end of reionization have the chance to form outside ionized bubbles and start their star formation activity. In the model with $f_{\rm esc} = 0.2$ and $v_c^* = 50$ km s$^{-1}$, the reionization completes at $z_{\rm re} = 6.6$. Haloes formed before $z_{\rm re}$ shine only due to their relic stars, and fade away with time; in haloes with $v_c > v_c^*$, most UV radiation is continuously supplied by newly formed stars. As a result, there is a gap in the LFs corresponding to these two (physically distinct) halo populations, and the gap broadens with time.

The number of faint galaxies starts to deviate from the no-feedback model significantly only in the late stages of reionization (EoR lasts for ∼300–600 Myr), because earlier on the time stretch is too short to suppress star formation in most haloes. By varying the $f_{\rm esc}$, one can change the reionization history. For instance, if we decrease $f_{\rm esc}$ to 0.1 (yielding $z_{\rm re} = 6.0$), as shown in Fig. 7, faint galaxies with $M_{\rm UV,obs} \gtrsim -9$ could have abundance higher than galaxies as bright as $M_{\rm UV,obs} \sim -18$.

For comparison, the LFs from hydrodynamical simulations combined with radiative transfer calculation in Wise et al. (2014) and in Gnedin (2016) are also shown in the corresponding panels for the same (or very similar) redshifts in Fig. 6. We find that at redshift 6 and 7, the Gnedin (2016) LFs are close to our model with $v_c^* = 30$ km s$^{-1}$, however at redshift 8 we predict more faint galaxies above the turnover UV magnitudes than Gnedin (2016). On the other hand, the Wise et al. (2014) LFs are always similar to our no-feedback models.

To get a deeper insight, we plot separately the LFs of haloes with $v_c > v_c^*$ and with $v_c < v_c^*$ at different redshifts in Fig. 8, for $v_c^* = 30$ and 50 km s$^{-1}$, respectively. Also shown are the available observational data from Bouwens et al. (2015a). From the figure we clearly see how reionization feedback gradually separates the two components inducing an increasing deviation from the no-feedback LF reference model. It is worthwhile noting that although we just simply adopt a constant circular velocity threshold as a star formation quenching criterion, the LFs have rather complex behaviours at the faintest end. From $z \sim 8$ to $z \sim 5$, the abundance of galaxies with $M_{\rm UV,obs} > M^*_{\rm UV,obs}$ evolves fast, and these faint galaxies hosted by haloes with $v_c < v_c^*$ become EoR relics (see e.g. Ricotti & Gnedin 2005; Salvadori & Ferrara 2009; Benítez-Llambay et al. 2015).

The above discussions are only concerned with the $f(M_h)$ calibrated by using best-fitting Schechter parameters. Considering the uncertainties, predictions on the number of galaxies at the faint-end ($M_{\rm UV,obs} \gg M^*_{\rm UV,obs}$) are rather uncertain, as shown by shaded regions in each panel of Figs 6 and 7. On the other hand, the observed abundance of ultra-faint galaxies can put tight limits on the star formation efficiency of small haloes.

### 3.3 Feedback imprints on galaxy properties

We further investigate the imprints of reionization feedback on galaxies properties. The first is the $M_{\rm UV,obs} - M_{\rm h}$ relation, which

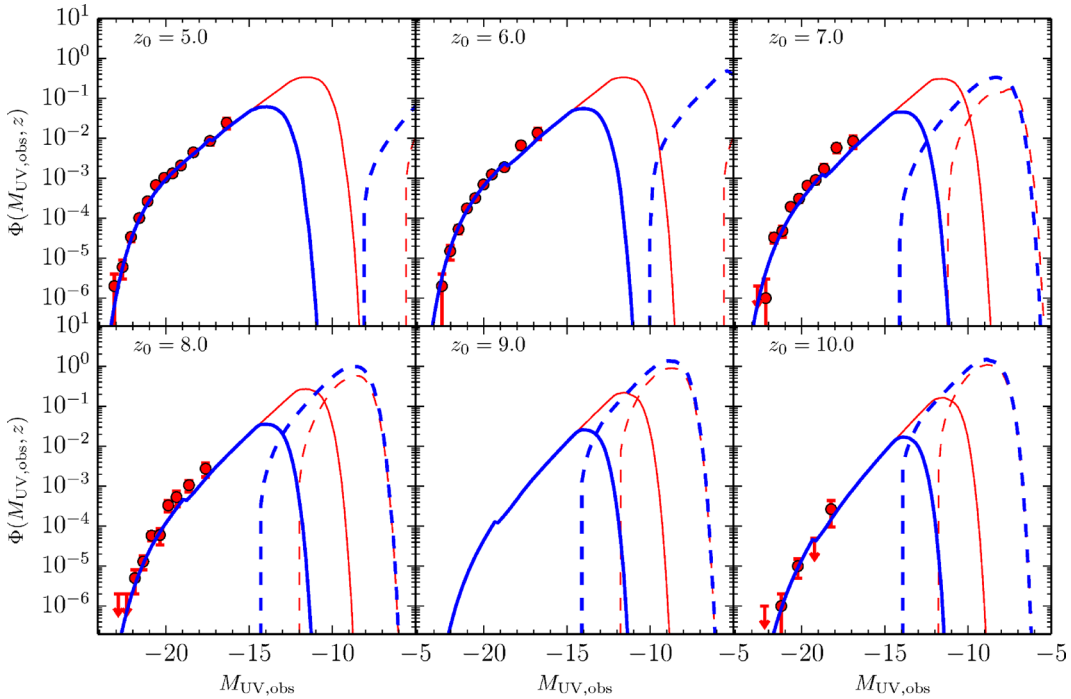


**Figure 8.** The contributions from haloes with $v_c < v_c^*$ (dashed) and $v_c > v_c^*$ (solid) to the predicted LFs at different redshifts for models with $v_c^* = 30$ (thin) and 50 km s$^{-1}$ (thick), respectively. To highlight the difference between these two components, uncertainties are not shown.

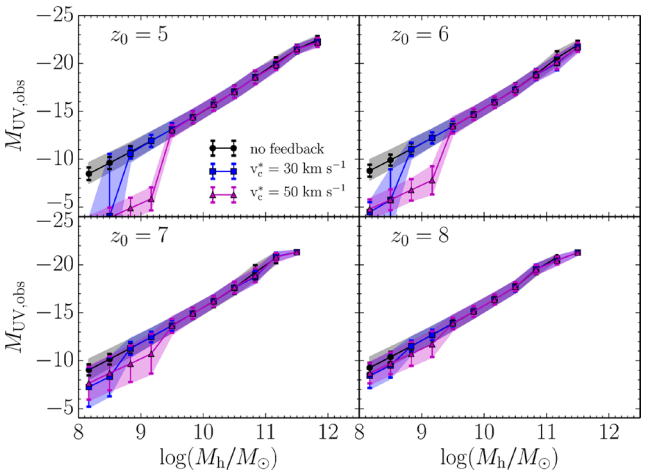


**Figure 9.** The $M_{\rm UV,obs} - M_{\rm h}$ relations for haloes at redshifts 5, 6, 7 and 8 in models with $v_c^* = 30$ and 50 km s$^{-1}$, and in no-feedback model, respectively. Errorbars are the intrinsic scatters of the absolute UV magnitudes in each halo mass bin, while the shaded regions are the full uncertainties including both the intrinsic scatters and the uncertainties in calibrating the $f(M_{\rm h})$.

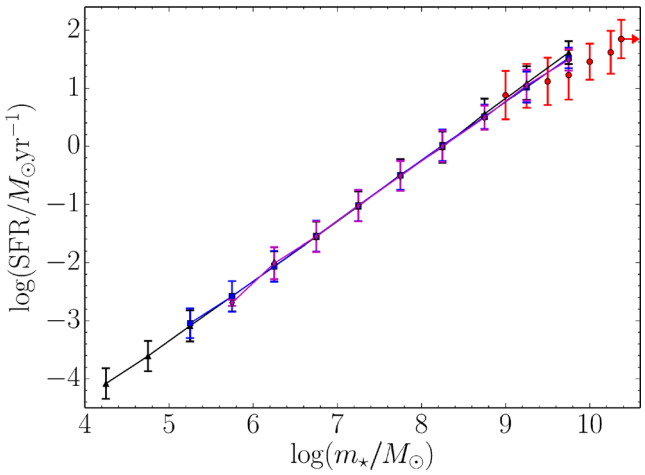


**Figure 10.** The SFR versus $m_\star$ and the corresponding uncertainties at redshift 5 for three models respectively. For comparison we also plot the observed relation in Salmon et al. (2015). We only show the intrinsic scatters because in the SFR–$m_\star$ relation the uncertainties due to calibrating star formation efficiency is very small and scarcely visible.

critically concerns the galaxy LFs discussed above. As different halo mass assembly histories introduce an intrinsic scatter in this relation, in order to derive the scatter, it is more appropriate to generate Monte Carlo random samples. The samples are generated by using the probability distribution of the (a) halo mass (given by the halo mass function), (b) formation time (from equation 11 for a given halo mass $M_{\rm h}$, and redshift $z_0$), and (c) quenching time (using $\propto d\mathcal{P}_b/dz_q$ and $z_0 < z_q < z_f$) obtained above. In Fig. 9 we show the results at redshifts 5, 6,7 and 8, for the no-feedback reference model, and for $v_c^* = 30$ and 50 km s$^{-1}$. All models have $f_{\rm esc} = 0.2$. We use the error bars to represent the intrinsic scatter of the absolute UV magnitudes due to different mass assembly histories of haloes in the same mass bin and due to different reionization imprints on them, and shaded regions to represent the full uncertainties considering both the intrinsic scatters and the uncertainties in calibrating the star formation efficiency. The reionization feedback decreases the mean luminosity of haloes with $v_c < v_c^*$ at the same time increasing the scatter, imprinting an ankle-knee feature in the relation.

We also extract the SFR–$m_*$ and $t_*$–$M_{\rm UV,obs}$ relations from the above Monte Carlo samples. The SFR–$m_\star$ relation at $z_0 = 5$ is shown in Fig. 10, and compared with data from Salmon et al. (2015). Our predicted SFR–$m_\star$ relations agree well with observations in the overlapping $m_\star$ range. Discrepancies in the SFR–$m_\star$ relations of the three models are modest at $m_\star \gtrsim 10^6$ M$_\odot$; however,

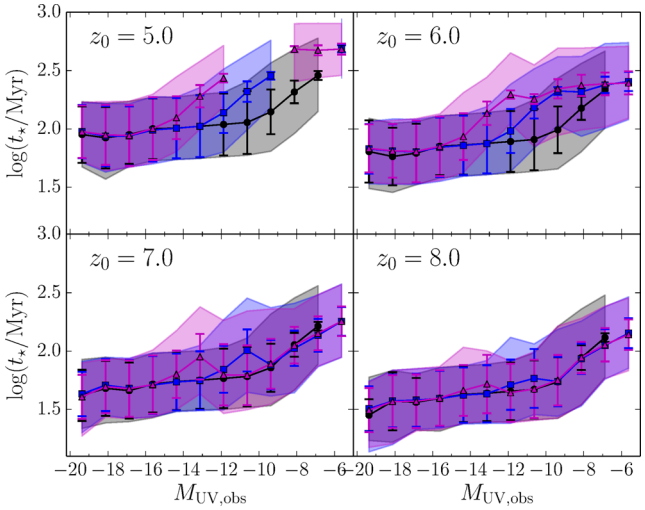


**Figure 11.** The $t_\star$ - $M_{\mathrm{UV,obs}}$ relations and the corresponding uncertainties at redshifts 5, 6, 7 and 8 respectively. Same to Fig. 9, errorbars mean the intrinsic scatters while the shaded regions mean the full uncertainties.

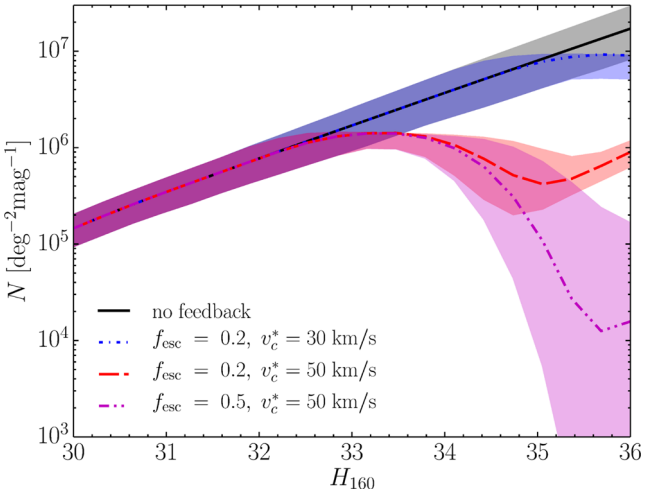


**Figure 12.** The predicted number counts of galaxies with $z = 5$–8 in models with different parameters.

in the $v_c^* = 30$ (50) km s$^{-1}$ models star formation in all galaxies with $m_\star \lesssim 10^5(10^6)\,\mathrm{M}_\odot$ has already been quenched before redshift 5. The SFR–$m_\star$ relations at higher redshifts have a similar trend, except that the amplitudes increase by about 0.1 dex per redshift.

The analogous stellar age ($t_\star$) versus $M_{\mathrm{UV,obs}}$ relation is plotted in Fig. 11. We find that at redshift 5 galaxies with $M_{\mathrm{UV,obs}} \lesssim -16$ have mean stellar age ∼100 Myr. Above this absolute UV magnitude models start to diverge, with stronger feedback models predicting relatively older galaxies. By looking at the $t_\star$–$M_{\mathrm{UV,obs}}$ relations it is easier to distinguish models in the range $-13 \lesssim M_{\mathrm{UV,obs}} \lesssim -8$. Therefore, stellar age measurements of galaxies in this range could be used as a probe of reionization feedback strength. At higher redshifts stars are typically younger: for example at $z = 8$ galaxies with $M_{\mathrm{UV,obs}} < -10$ are about 30 Myr old.

### 3.4 Feedback imprints on galaxy counts

We have pointed that our model predicts a Thomson optical depth $\tau$ consistent with the *Planck* constraints in a wide $v_c^*$ range. Therefore this indirect observation is not very helpful in discriminating models with different $v_c^*$. However, at the faintest magnitudes different models predict substantially different galaxy number counts in a given redshift range from $z_1$ to $z_2$,

$$N(H_{160}) = \int_{z_1}^{z_2} r^2 \Phi(M_{\mathrm{UV,obs}}, z) \frac{\mathrm{d}r}{\mathrm{d}z} \mathrm{d}z, \tag{28}$$

where $H_{160}$ is the apparent magnitude observed at 1.6 μm, corresponding to rest-frame luminosity at $1.6/(1+z)$ μm. This rest-frame luminosity is converted to the absolute UV magnitude at 1600 Å using the $l_\nu(\Delta t)$ as in equation (6), but at fixed $\Delta t = 100$ Myr for convenience. Hence, number count observations could directly put constraints on $v_c^*$, as shown in Fig. 12 for galaxies in the redshift range 5–8. Among these ultra-faint galaxies a substantial fraction of them are located in $z = 7$–8, due to the steeper slope of the LF at $z \sim 8$ compared to at $z \sim 5$. For example, we check that for the number count of no-feedback model shown in Fig. 12, at $H_{160} \sim 30$ about ∼16 per cent is in $z = 7$–8, at $H_{160} \sim 36$ this fraction is ∼25 per cent. Existing and/or forthcoming galaxy surveys are unlikely to reach the very deep limiting magnitudes required. However, if gravitational lensing (e.g. Yue et al. 2014) can be exploited, it is possible to detect a handful of ultra-faint galaxies, that would allow us to put tight constraints on feedback strength. The results of investigations using two Frontier Fields clusters are presented in Castellano et al. (2016).

## 4 CONCLUSIONS

The star formation activity in small haloes with shallow gravitational potential well is easily quenched by external ionizing flux from nearby sources and/or an ionizing radiation background. Such quenching effect might play a significant role in shaping the reionization history, when more and more galaxies formed in/entered into ionized bubbles whose size keeps growing throughout the EoR. Thereby the LF of such faint galaxies provides key information on the interplay between the reionization process and its driving sources.

We have investigated the LF of faint galaxies during the EoR by including the above reionization feedback in an analytical model. The model derives the LF from halo mass function by constructing luminosity–halo mass relations from observationally calibrated star formation efficiency and halo mass assembly history. Reionization feedback effects are included by adopting a constant threshold circular velocity, $v_c^*$, below which the star formation of haloes located in ionized bubbles is quenched. We computed the LFs for models with different $f_{\mathrm{esc}}$ and $v_c^*$ values, and found the following.

(i) If reionization feedback is neglected, the power-law Schechter parametrization characterizing the faint-end of the LF remains valid up to $M_{\mathrm{UV,obs}}^* \sim -9$ (corresponding to the atomic-cooling haloes mass, see Appendix A for an estimate of supernova explosion effects). Above this absolute UV magnitude the number density of galaxies drops dramatically.

(ii) When feedback is included, small haloes ($v_c < v_c^*$) in ionized bubbles fail to collect enough gas to ignite/sustain their star formation. The reionization history, constrained by the *Planck* electron scattering optical depth, is insensitive to $v_c^*$.

(iii) For strong feedback, i.e. $v_c^* = 50$ km s$^{-1}$, the LF deviates from the Schechter function above $M_{\mathrm{UV,obs}}^* \sim -15$, slightly below the detection limit of current surveys of blank fields at $z \sim 5$ (Bouwens et al. 2015a). Hence, we expect that upcoming observations will obtain important constraints on $v_c^*$.

(iv) In addition, even for strong feedback, the LF may rise again at luminosities fainter than $M^*_{\rm UV,obs}$ as a result of the interplay between reionization process and galaxy formation.

(v) We also pointed out that the $t_\star$–$M_{\rm UV}$ relation might be used as a powerful probe of reionization feedback strength. In models with stronger reionization feedback, stars in galaxies with $-13 \lesssim M_{\rm UV,obs} \lesssim -8$ are typically older. Other constraints on $f_{\rm esc}$ and $v_c^*$ in our model, can come from galaxy number count data, particularly from those exploiting gravitational lensing magnification.

Our model contains some necessary simplifications and assumptions. The most relevant one is perhaps the use of a constant circular velocity threshold as the criterion for quenching star formation, and its treatment as a free parameter independent of $f_{\rm esc}$. This is a standard assumption in the literature and is very convenient when performing analytical calculations. Instead, detailed simulations (e.g. Sobacchi & Mesinger 2013b) pointed out that in the presence of reionization feedback, the gas fraction decreases gradually as the halo mass decreases, following a relation $2^{-M_c/M_{\rm h}}$, where $M_c$ is a critical halo mass. We believe that this effect would make the LF smoother around the turnover point and may result in more faint galaxies. However, we do not expect significant changes in the basic trend of the galaxy LF found here.

In our work, we take the model parameters that give predictions consistent with the direct observations of the LFs at $z > 5$ in the blank fields. There are alternative ways to investigate the reionization feedback and constrain the high-$z$ LFs using indirect observations. At intermediate redshifts ($2 \lesssim z \lesssim 5$) the IGM is fully ionized and a global ionizing UV background is in place. Hence the radiative feedback effects should be maximal. The known existence of faint galaxies in these epochs implies the existence of even more fainter galaxies in the EoR.

For example, in Alavi et al. (2014) the observations of galaxies at $z \sim 2$ confirm the validity of the Schechter formula down to absolute UV magnitude $\sim -13$. These results show that such faint galaxies support active star formation well after the EoR. As a consequence, it is likely that $v_c^* \lesssim 50$ km s$^{-1}$ if we incorporate this information into our model.

In addition, the number of ultra-faint satellites in the Local Group also put constraints on the faint-end of the EoR LF once used in combination with their merger tree history, see Weisz, Johnson & Conroy (2014), Boylan-Kolchin, Bullock & Garrison-Kimmel (2014), Boylan-Kolchin et al. (2015). Finally, the rate of high-$z$ GRBs is another probe of the abundance of ultra-faint galaxies in the EoR (Trenti et al. 2012). Here, we checked that distinguishing models with different $v_c^*$ requires very high precision measurements of the star formation rate density (SFRD). Even at $z \sim 5$ the SFRD difference between the no-feedback model and the $v_c^* = 50$ km s$^{-1}$ is only about 10 per cent, i.e. much smaller than the current precision of the SFRD derived from GRB observations. Nevertheless, all these alternative techniques nicely complement investigations, as the one presented here, based on direct LFs or number count data.

## ACKNOWLEDGEMENTS

YX is supported by the NSFC grant 11303034, and the Young Researcher Grant of National Astronomical Observatories, Chinese Academy of Sciences.

## REFERENCES

Abel T., Bryan G. L., Norman M. L., 2002, Science, 295, 93
Alavi A. et al., 2014, ApJ, 780, 143
Atek H. et al., 2015, ApJ, 800, 18
Barkana R., Loeb A., 2001, Phys. Rep., 349, 125
Becker R. H. et al., 2001, AJ, 122, 2850
Behroozi P. S., Silk J., 2015, ApJ, 799, 32
Benítez-Llambay A., Navarro J. F., Abadi M. G., Gottlöber S., Yepes G., Hoffman Y., Steinmetz M., 2015, MNRAS, 450, 4207
Bouwens R. J. et al., 2011, ApJ, 737, 90
Bouwens R. J. et al., 2014, ApJ, 793, 115
Bouwens R. J. et al., 2015a, ApJ, 803, 34
Bouwens R. J. et al., 2015b, preprint (arXiv:1506.01035)
Boylan-Kolchin M., Bullock J. S., Garrison-Kimmel S., 2014, MNRAS, 443, L44
Boylan-Kolchin M., Weisz D. R., Johnson B. D., Bullock J. S., Conroy C., Fitts A., 2015, MNRAS, 453, 1503
Bromm V., Yoshida N., Hernquist L., McKee C. F., 2009, Nature, 459, 49
Bruzual G., Charlot S., 2003, MNRAS, 344, 1000
Castellano M. et al., 2016, ApJ, 823, L40
Cen R., Ostriker J. P., 1992, ApJ, 399, L113
Chiu W. A., Ostriker J. P., 2000, ApJ, 534, 507
Choudhury T. R., Ferrara A., 2007, MNRAS, 380, L6
Choudhury T. R., Srianand R., 2002, MNRAS, 336, L27
Ciardi B., Ferrara A., 2005, Space Sci. Rev., 116, 625
Dayal P., Ferrara A., Dunlop J. S., Pacucci F., 2014, MNRAS, 445, 2545
Dijkstra M., Haiman Z., Rees M. J., Weinberg D. H., 2004, ApJ, 601, 666
Eisenstein D. J., Hu W., 1998, ApJ, 496, 605
Ellis R. S. et al., 2013, ApJ, 763, L7
Fan X., Carilli C. L., Keating B., 2006, ARA&A, 44, 415
Ferrara A., Loeb A., 2013, MNRAS, 431, 2826
Finkelstein S. L., 2015, preprint (arXiv:1511.05558)
Finkelstein S. L. et al., 2012, ApJ, 758, 93
Finkelstein S. L. et al., 2015, ApJ, 810, 71
Furlanetto S. R., Hernquist L., Zaldarriaga M., 2004a, MNRAS, 354, 695
Furlanetto S. R., Zaldarriaga M., Hernquist L., 2004b, ApJ, 613, 1
Giocoli C., Moreno J., Sheth R. K., Tormen G., 2007, MNRAS, 376, 977
Gnedin N. Y., 1996, ApJ, 456, 1
Gnedin N. Y., 2000, ApJ, 542, 535
Gnedin N. Y., 2016, ApJ, 825, L17
Iliev I. T., Mellema G., Shapiro P. R., Pen U.-L., 2007, MNRAS, 376, 534
Illingworth G. D. et al., 2013, ApJS, 209, 6
Jaacks J., Choi J.-H., Nagamine K., Thompson R., Varghese S., 2012, MNRAS, 420, 1606
Kitayama T., Tajiri Y., Umemura M., Susa H., Ikeuchi S., 2000, MNRAS, 315, L1
Leitherer C. et al., 1999, ApJS, 123, 3
Leitherer C., Ortiz Otálvaro P. A., Bresolin F., Kudritzki R.-P., Lo Faro B., Pauldrach A. W. A., Pettini M., Rix S. A., 2010, ApJS, 189, 309
Livermore R. C., Finkelstein S. L., Lotz J. M., 2016, preprint (arXiv:1604.06799)
Lorenzoni S., Bunker A. J., Wilkins S. M., Stanway E. R., Jarvis M. J., Caruana J., 2011, MNRAS, 414, 1455
McLeod D. J., McLure R. J., Dunlop J. S., 2016, MNRAS, 459, 3812
McLure R. J. et al., 2013, MNRAS, 432, 2696
Mashian N., Oesch P. A., Loeb A., 2016, MNRAS, 455, 2101
Mason C., Trenti M., Treu T., 2015, ApJ, 813, 21
Meurer G. R., Heckman T. M., Calzetti D., 1999, ApJ, 521, 64
Mitra S., Choudhury T. R., Ferrara A., 2015, MNRAS, 454, L76
Muñoz J. A., Loeb A., 2011, ApJ, 729, 99
Naoz S., Noter S., Barkana R., 2006, MNRAS, 373, L98
O'Shea B. W., Wise J. H., Xu H., Norman M. L., 2015, ApJ, 807, L12
Oesch P. A. et al., 2013, ApJ, 773, 75
Oesch P. A. et al., 2014, ApJ, 786, 108
Ouchi M. et al., 2010, ApJ, 723, 869
Pallottini A., Ferrara A., Gallerani S., Salvadori S., D'Odorico V., 2014, MNRAS, 440, 2498
Planck Collaboration XIII, 2015, preprint (arXiv:1502.01589)
Planck Collaboration XLVII, 2016, preprint (arXiv:1605.03507)
Ricotti M., Gnedin N. Y., 2005, ApJ, 629, 259
Roberts-Borsani G. W. et al., 2016, ApJ, 823, 143

Robertson B. E. et al., 2013, ApJ, 768, 71
Robertson B. E., Ellis R. S., Furlanetto S. R., Dunlop J. S., 2015, ApJ, 802, L19
Salmon B. et al., 2015, ApJ, 799, 183
Salvadori S., Ferrara A., 2009, MNRAS, 395, L6
Salvaterra R., Ferrara A., Dayal P., 2011, MNRAS, 414, 847
Samui S., Srianand R., Subramanian K., 2007, MNRAS, 377, 285
Sheth R. K., Tormen G., 1999, MNRAS, 308, 119
Sheth R. K., Mo H. J., Tormen G., 2001, MNRAS, 323, 1
Sobacchi E., Mesinger A., 2013a, MNRAS, 432, 3340
Sobacchi E., Mesinger A., 2013b, MNRAS, 432, 51
Stark D. P., Ellis R. S., Chiu K., Ouchi M., Bunker A., 2010, MNRAS, 408, 1628
Sun G., Furlanetto S. R., 2016, MNRAS, 460, 417
Tacchella S., Trenti M., Carollo C. M., 2013, ApJ, 768, L37
Thoul A. A., Weinberg D. H., 1996, ApJ, 465, 608
Tornatore L., Ferrara A., Schneider R., 2007, MNRAS, 382, 945
Trenti M., Stiavelli M., 2007, ApJ, 667, 38
Trenti M., Stiavelli M., Bouwens R. J., Oesch P., Shull J. M., Illingworth G. D., Bradley L. D., Carollo C. M., 2010, ApJ, 714, L202
Trenti M., Perna R., Levesque E. M., Shull J. M., Stocke J. T., 2012, ApJ, 749, L38
Vázquez G. A., Leitherer C., 2005, ApJ, 621, 695
Weisz D. R., Johnson B. D., Conroy C., 2014, ApJ, 794, L3
Wise J. H., Demchenko V. G., Halicek M. T., Norman M. L., Turk M. J., Abel T., Smith B. D., 2014, MNRAS, 442, 2560
Wyithe J. S. B., Loeb A., Oesch P. A., 2014, MNRAS, 439, 1326
Yue B., Ferrara A., Vanzella E., Salvaterra R., 2014, MNRAS, 443, L20

## APPENDIX A: SUPERNOVA FEEDBACK

The star formation efficiency is calibrated by assuming that the Schechter parametrization for LFs always holds down to the atomic-cooling halo mass. This might not be true for small haloes in which gas could be totally blown away by supernova explosion, therefore in this section we have a check on it. Haloes can sustain the continuous star formation mode if the energy deposited by supernova explosions does not exceed the gravitational binding energy of the halo,

$$m_\star \eta_{\rm SN} E_{\rm SN} < \frac{1}{2} M_{\rm h} f_{\rm g} v_{\rm esc}^2 = M_{\rm h} f_{\rm g} v_c^2, \quad \text{(A1)}$$

where $E_{\rm SN}$ is the energy released by supernova per stellar mass and $\eta_{\rm SN} \sim 0.1$ (Pallottini et al. 2014) is the fraction that this energy goes into the gas, $f_{\rm g}$ is the gas fraction and $v_{\rm esc} = \sqrt{2} v_c$ is the escape velocity. In our case $m_\star \approx M_{\rm h} f(M_{\rm h})/2$, we have

$$f(M_{\rm h}) \lesssim \frac{2 f_{\rm g} v_c^2}{\eta_{\rm SN} E_{\rm SN}}. \quad \text{(A2)}$$

If the upper limit at the right hand side is smaller than the calibrated star formation efficiency the halo has to adjust itself to have the new star formation efficiency satisfies the equation (A2) (Dayal et al. 2014). Simply assuming $f_{\rm g} = \Omega_b/\Omega_m$, and taking $E_{\rm SN}$ from the outputs of STARBURST99[5] (Leitherer et al. 1999; Vázquez & Leitherer 2005; Leitherer et al. 2010, for consistence reason we also replace the $l_\nu(\Delta t)$ in equation (6) with the one from STARBURST99 in this check), we check that for the Salpeter IMF with the mass ranges of 0.1–100 $M_\odot$, 1–100 $M_\odot$ and 3–150 $M_\odot$, the equation (A2) always holds for halo mass above the atomic-cooling mass, as long as $\eta_{\rm SN} \lesssim 0.4$ when the metallicity is $0.02\,Z_\odot$, and as long as $\eta_{\rm SN} \lesssim 0.3$ when the metallicity is $2\,Z_\odot$. We therefore believe that our assumption is safe enough. This is because in our work for any given metallicity and IMF, we calibrate the corresponding $f(M_{\rm h})$ to reproduce the observed LF at $z_0 \sim 5$. In the IMF models with more massive stars, both the $E_{\rm SN}$ and the $l_\nu(\Delta t)$ are higher. The higher $l_\nu(\Delta t)$ consequently results in a smaller $f(M_{\rm h})$, limiting the total energy released by supernovae $\propto f(M_{\rm h})\eta_{\rm SN} E_{\rm SN}$, so the host haloes could still hold the star formation activity. The effects by Pop III stars are not considered here, as pointed by numerical simulations (Tornatore, Ferrara & Schneider 2007; Pallottini et al. 2014) Pop III stars are negligible in haloes above the atomic-cooling criterion.

[5] http://www.stsci.edu/science/starburst99/docs/default.htm

## APPENDIX B: $\mathcal{P}_{\rm b}$ VERSUS $Q_{\rm H\,II}$

We integrate equation (4) in Furlanetto, Hernquist & Zaldarriaga (2004a) to calculate the probability that a halo sits in ionized bubbles above a minimum size. This is basically an application of the 'bubble model' scenario discussed in Furlanetto, Zaldarriaga & Hernquist (2004b). The minimum bubble size is set by requiring that a target halo has at least one neighbour with $v_c > v_c^*$ within the bubble radius. Namely, we have the two-point halo correlation function:

$$\xi_h(m_1, m_2, r, z) = \xi(r, z) b(m_1, z) b(m_2, z), \quad \text{(B1)}$$

where $\xi$ is the matter two-point correlation function and $b$ is the halo bias (Sheth et al. 2001). We then obtain the number of neighbouring haloes within radius $d$ and above $M^*$

$$N = \int_{<d} 4\pi r^2 {\rm d}r \int_{>M^*} [1 + \xi_h(r, z, m_1, M_h)] \frac{{\rm d}n}{{\rm d}M_{\rm h}} {\rm d}M_{\rm h}; \quad \text{(B2)}$$

$d$ is then determined by solving the above equation for $N = 1$.

The bubble model uses the cumulative ionizing photons number per collapsed atom, $\zeta$, to calculate $\mathcal{P}_b$, but this number is not explicitly appearing in our algorithm. However, we find that although the reionization history depends on $\zeta$, if we plot the $\mathcal{P}_b$ as a function of $\zeta f_{\rm coll}$ ($\sim Q_{\rm H\,II}$), where $f_{\rm coll}$ is the collapse fraction, we actually see limited variations in a large $\zeta$ range (see different curves in Fig. B1). Therefore, in this paper we adopt the following approximation: when calculating the $\mathcal{P}_b$ we fix $\zeta = 10$ and take the $\mathcal{P}_b$ value at the time at which $\zeta\, f_{\rm coll} = Q_{\rm H\,II}$. The above algorithm does not take into account the dependence of $\mathcal{P}_b$ on the halo formation redshift, $z_f$. Haloes formed earlier are more biased, therefore they might have higher probability to be located in the ionized bubbles. This improvement will be deferred to future work.

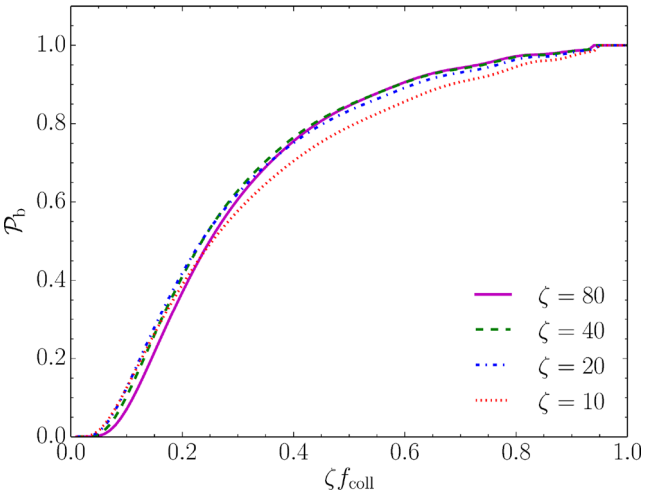


**Figure B1.** The $\mathcal{P}_{\rm b}$ for $M_{\rm h} = 10^9\,M_\odot$ as a function of $\zeta f_{\rm coll}$ for different $\zeta$.

This paper has been typeset from a TEX/LATEX file prepared by the author.